

## Original Research Article

## Artificial intelligence-based automated segmentation and radiotherapy dose mapping for thoracic normal tissues

Jue Jiang<sup>a,1</sup>, Chloe Min Seo Choi<sup>a,c,1</sup>, Joseph O. Deasy<sup>a</sup>, Andreas Rimner<sup>b</sup>, Maria Thor<sup>a,\*</sup>, Harini Veeraraghavan<sup>a,\*</sup><sup>a</sup> Department of Medical Physics, Memorial Sloan Kettering Cancer Center, New York, NY, United States<sup>b</sup> Department of Radiation Oncology, Memorial Sloan Kettering Cancer Center, New York, NY, United States<sup>c</sup> Department of Radiation Oncology, Yonsei Cancer Center, Heavy Ion Therapy Research Institute, Yonsei University College of Medicine, Seoul, South Korea

## ARTICLE INFO

## Keywords:

Artificial intelligence  
Registration-segmentation  
Automated dose mapping  
Lung cancer  
CBCT

## ABSTRACT

**Background and purpose:** Objective assessment of delivered radiotherapy (RT) to thoracic organs requires fast and accurate deformable dose mapping. The aim of this study was to implement and evaluate an artificial intelligence (AI) deformable image registration (DIR) and organ segmentation-based AI dose mapping (AIDA) applied to the esophagus and the heart.

**Materials and methods:** AIDA metrics were calculated for 72 locally advanced non-small cell lung cancer patients treated with concurrent chemo-RT to 60 Gy in 2 Gy fractions in an automated pipeline. The pipeline steps were: (i) automated rigid alignment and cropping of planning CT to week 1 and week 2 cone-beam CT (CBCT) field-of-views, (ii) AI segmentation on CBCTs, and (iii) AI-DIR-based dose mapping to compute dose metrics. AIDA dose metrics were compared to the planned dose and manual contour dose mapping (manual DA).

**Results:** AIDA required ~2 min/patient. Esophagus and heart segmentations were generated with a mean Dice similarity coefficient (DSC) of  $0.80 \pm 0.15$  and  $0.94 \pm 0.05$ , a Hausdorff distance at 95th percentile (HD95) of  $3.9 \pm 3.4$  mm and  $14.1 \pm 8.3$  mm, respectively. AIDA heart dose was significantly lower than the planned heart dose ( $p = 0.04$ ). Larger dose deviations ( $\geq 1$  Gy) were more frequently observed between AIDA and the planned dose ( $N = 26$ ) than with manual DA ( $N = 6$ ).

**Conclusions:** Rapid estimation of RT dose to thoracic tissues from CBCT is feasible with AIDA. AIDA-derived metrics and segmentations were similar to manual DA, thus motivating the use of AIDA for RT applications.

## 1. Introduction

Locally advanced non-small cell lung cancers (LA-NSCLC) regress over the radiotherapy (RT) course [1,2]. It has been shown that the estimate of spill over RT dose to the thoracic normal tissues computed using deformable image registration (DIR) dose mapping often deviates from the planned dose snapshot from the pre-treatment anatomy [3,4]. Furthermore, inadequate normal tissue segmentations may contribute to normal tissue overdosage and deteriorate the effectiveness of treatments including clinical trials [5]. However, accurate, fast, and automated registration and segmentation solutions are crucial to accumulate dose [6] and enable treatment adaptation [2,7] informed by tumor shrinkage patterns [8,9] and early indications of radiation-induced normal tissue toxicity [3,10] to be useful in clinical settings.

Iterative DIR methods have demonstrated the ability to deformably map the dose from the planning CT (pCT) and to accumulate normal tissue doses from during-treatment cone-beam CTs (CBCT) [3,11]. However, iterative DIR methods may require manual specification and tuning of registration parameters. In addition, the presence of large anatomical deformations often reduces the accuracy of such methods, diminishing their use for clinical dose warping and/or dose accumulation. Prior works have shown that accurate alignment is possible when combining manually delineated organs into the registration of CTs [12,13] as well as CBCTs [11,14–16].

Our previously developed approach, ‘patient-specific anatomic context and shape’ (PACS) [17], improves on prior methods by combining automated segmentation and registration in a single network. The registration network within PACS provides spatially

\* Corresponding authors.

E-mail addresses: [thorm@mskcc.org](mailto:thorm@mskcc.org) (M. Thor), [veeraragh@mskcc.org](mailto:veeraragh@mskcc.org) (H. Veeraraghavan).<sup>1</sup> These authors have contributed equally to the work.

aligned geometries from prior scans to guide segmentation, while the segmentation network provides contour guidance to improve deformable alignment. Hence, PACS does not require manual delineation thus allowing an automated pipeline. Furthermore, PACS does not require computationally expensive multi-stage analysis pipeline [18] or additional processing to generate synthetic CT images to compute alignment [19]. Also unlike single-step deep learning (DL) registration [19,20], PACS progressively refines registration and segmentation via 3D convolutional long short-term memory (3D-CLSTM) in the encoder layers, thus modelling a spatially and temporally varying deformation field to handle large deformations. In this study, our prior work applied to the longitudinal segmentation of lung tumors and the esophagus [16] is extended by, (i) performing dose mapping on weekly CBCT, (ii) using a fully automatic analysis pipeline to segment organs and deforming images for dose mapping, and (iii) applying automated artificial intelligence dose mapping (AIDA) to both esophagus and the heart that is an additional development of our prior study that used manual segmentation and iterative DIR based dose accumulation for the esophagus alone [3,11].

The aims of this study were to implement and evaluate AI automated dose mapping to thoracic organs, and compare AIDA-derived dose with the planned dose and manual contour-based dose mapping (manual DA).

## 2. Materials and methods

### 2.1. Cohort

This retrospective analysis study was approved by the local institutional review board at the Memorial Sloan Kettering Cancer Center. The analyzed cohort consisted of 72 LA-NSCLC patients treated with intensity-modulated RT to 60 Gy in 2 Gy fractions (Eclipse; Varian Medical Systems) and concurrent chemotherapy between June 2016 and March 2019 [3] that had a free-breathing pCT in addition to weekly CBCTs acquired during the first two weeks of RT (8 patients were excluded due to missing CBCT at either of the two time points). DIR was performed between the pCT and mid-phase CBCTs. The two-week time point was motivated by treatment adaptation feasibility within this time window given the 4-week RT course. Further cohort-specific details can be found elsewhere [3,11].

### 2.2. Deep learning model for automated deformable dose mapping

Unlike prior work where the dose mapping pipeline focused on aligning weekly CBCTs with manually delineated esophagus [3,21], AI-DIR was performed between the pCT and each of the CBCTs, resulting in a total of 144 registrations. The in-plane resolution of the pCT was  $1.17 \times 1.17 \times$  and  $0.98 \times 0.98 \times 3$  mm<sup>3</sup> for the CBCTs. The PACS method [17] was directly applied without re-optimization or patient-specific tuning to align the CBCTs with the corresponding pCT. The registration network was used to compute the deformation vector field (DVF) between the pCT and CBCTs for deformable dose mapping. The segmentation network within PACS generated organ segmentations on each CBCT (Fig. 1).

The pre-processing steps were: rigid alignment performed automatically using the registration method available in open-source software-Advanced Normalization Tools (ANTs), followed by cropping the pCT to the CBCT field-of-view (FOV) [22]. The ANTs rigid registration was performed using mutual information as image matching loss, with an iteration step of 1000 and convergence threshold of  $1e-6$ . PACS consists of 3D-CLSTM networks implemented into the encoder layers of both registration and segmentation networks to handle large anatomy changes between pCT and CBCT scans. The segmentation and registration networks interact with each other, such that the incrementally refined alignments of the pCT produced by the registration network are used to provide a spatially aligned image prior to segmenting the CBCT scan. In this project, AIDA was implemented on a workstation with Intel Xeon 6248R Processor (3.0 GHz with 64 RAM). The time required to complete AIDA was measured. AIDA was compared against a reference dose mapping computed using manual segmentations of the same structures but utilizing the PACS-aware registration for dose propagation (manual DA) as well as planned dose to the organs. The PACS and AIDA pipeline will be made available through open-source GitHub upon manuscript acceptance for publication.

### 2.3. Registration accuracy, and dose comparisons

Deformable and voxel-wise dose mapping was performed by resampling the dose grid in the pCT coordinates to the CBCT coordinates using DVF after scaling the dose map in the planning coordinate to 6 weeks. The planned dose in each week was deformably mapped to the CBCTs from which the mean esophageal dose for week 1 (MEDw1) and

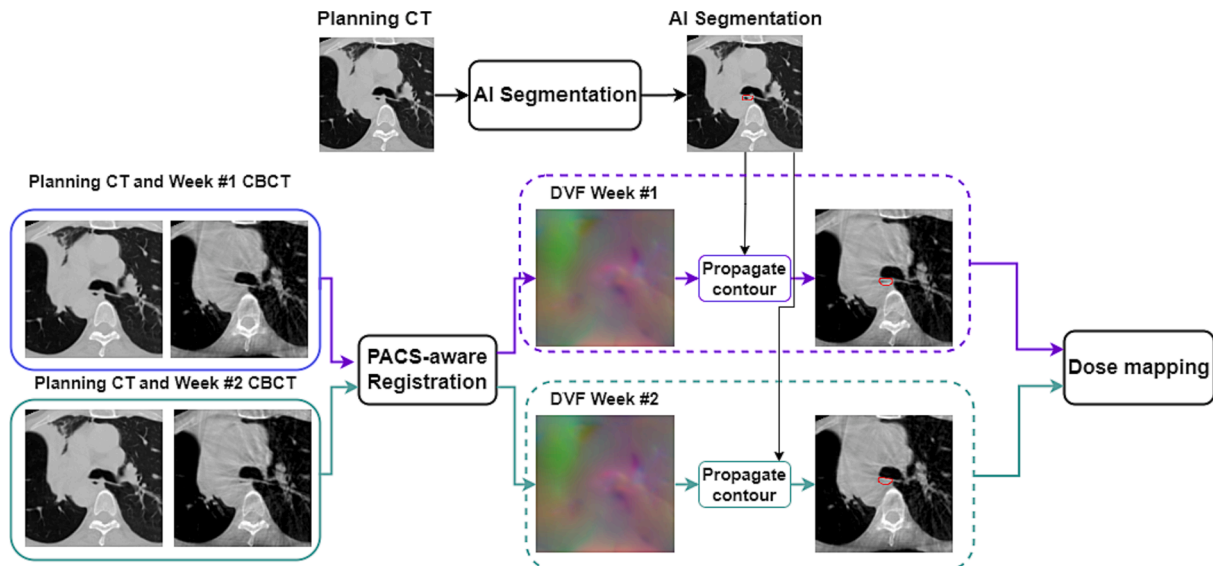


Fig. 1. AIDA overview. The AI-based AIDA pipeline uses AI DIR to deformably align the pCT to the weekly CBCTs as well as generate automated segmentation for organ dose mapping. Sample segmentation for the esophagus is shown.

planned dose mapped to week 2 CBCT were computed. A summary measure of MED<sub>w2</sub> was computed by adding the mean esophageal deformed dose at week 2 with MED<sub>w1</sub> using the segmented esophagus. Manual DA used manually delineated esophagus on the CBCT. AIDA used the PACS method to deform the planned doses to the CBCTs. The clinically delineated contours on pCT were used to provide spatially aligned geometries by the registration method to the segmentation subnetwork within PACS, which then generated tissue segmentation on the CBCT scans. The AIDA-derived doses were compared against planned doses and manual DAs using the Wilcoxon signed-rank test. The accuracy of dose estimation using the proposed model was compared against a publicly available iterative registration called Symmetric image normalization method (SyN) [23] that uses intensity-based DIR via B-splines.

Fully automated AIDA-based dose mapping was performed for the heart and esophagus in an 11-patient subset by propagating organ automatically segmented via AI on the pCT [24] with the PACS-aware registration [17]; the latter PACS registration subnetwork was used for propagating the dose maps. Heart segmentations were propagated because the published PACS model only segments the tumor and esophagus on the CBCT. More than 50 % of the superior-inferior extensions of the structures above were included in the FOV of the weekly CBCTs. The minimum dose to the hottest 90 % of the heart (heart D90) was assessed in addition to esophagus MED. The accuracy of AIDA was evaluated without any additional adjustments to the auto-segmentations.

#### 2.4. Statistical analysis

Geometric accuracies were computed from week 1 and week 2 CBCT using the Dice similarity coefficient (DSC), and the 95th percentile of the Hausdroff distance (HD95) that compared AI segmentations against manual delineations. Bland-Altman analysis was performed to compare the AI-generated and manually delineated volumes. Influence on dose was measured by comparing the MED and heart D90 doses produced using AIDA and manual DA. Bland-Altman analysis was also performed to compare cumulative mean dose differences to the esophagus using AIDA vs. manual DA or planned dose. In addition, 3D medial axis skeletons were computed [25] to measure the deviation of the medial axis skeletons between AI and manually segmented esophagus.

### 3. Results

#### 3.1. AIDA generated auto-segmentations for the esophagus were similar to manual delineations

Of the 72 analyzed patients, two patients had poor segmentations (DSC < 0.60), with one occurring at week 1 and a second at week 2. For the remaining 70 patients, the AIDA generated segmentations achieved an average DSC of  $0.80 \pm 0.15$  for week 1 and a DSC of  $0.82 \pm 0.10$  for week 2. The average HD95 was  $3.9 \pm 3.8$  mm and  $3.9 \pm 3.4$  mm for week 1 and week 2 CBCT scans, respectively. In comparison, SyN-based segmentation was significantly less accurate with a DSC of  $0.69 \pm 0.14$  ( $P < 0.001$ ) and a HD95 of  $7.2 \pm 6.0$  mm ( $P = 0.01$ ). AIDA segmentations showed a weak correlation between absolute MED deviation and DSC with an R-squared value of 0.03 and 0.07 respectively for week 1 and week 2 (Fig. 2). Only one patient had dose deviations exceeding 2 Gy (DSC = 0.63). SyN-derived doses exhibited large deviations even in cases with higher DSC. Notably, the deviation became more pronounced during week 2 for SyN, whereas AIDA was relatively comparable between weeks. On average, AIDA took 93 s to complete per patient, including the time required for rigid alignment of 90 s, cropping of 1 s, and DIR of 2 s.

Analysis of the differences in the medial axis skeletons of the AI from manually segmented esophagus was performed on the weekly CBCTs to identify regions with the most inferior segmentation performance. The distance between the medial axis skeletons in the individual slices was computed to determine the largest deviations in the segmentations. Deviations in medial axes ranged from 0.0 cm to 1.9 cm (mean:  $0.3 \pm 0.2$  cm) in week 1 and 0.0 cm to 1.7 cm (mean:  $0.3 \pm 0.3$  cm) in week 2 CBCT images.

AIDA demonstrated minimal impact on MED compared to manual delineations. Focusing on slices with the largest medial axis deviations between the AI segmented and manually delineated esophagus, the mean MED difference was  $5.4 \pm 3.4$  Gy and  $5.9 \pm 3.5$  Gy on week 1 and 2 CBCTs, respectively, with a maximum dose deviation of 10.9 Gy in both weekly CBCTs. Overall, MED<sub>w2</sub> measured across the whole esophagus volume was similar using both AIDA and manual DA (Fig. 3A), with an average difference of 0.4 Gy (range:  $-0.8, 1.6$  Gy). Fig. 3C shows Bland-Altman plots comparing the esophagus segmentations between AIDA vs. manual DA: the mean volume difference was  $-1.4$  cm<sup>3</sup> (range:  $-12.0, 9.2$  cm<sup>3</sup>) indicating that the AI-generated esophagus were smaller than the manually delineated esophagus.

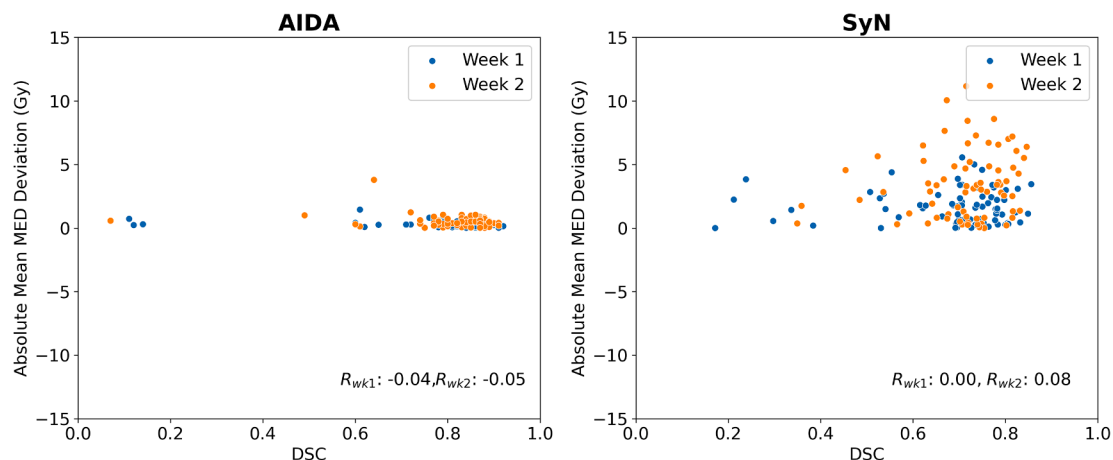
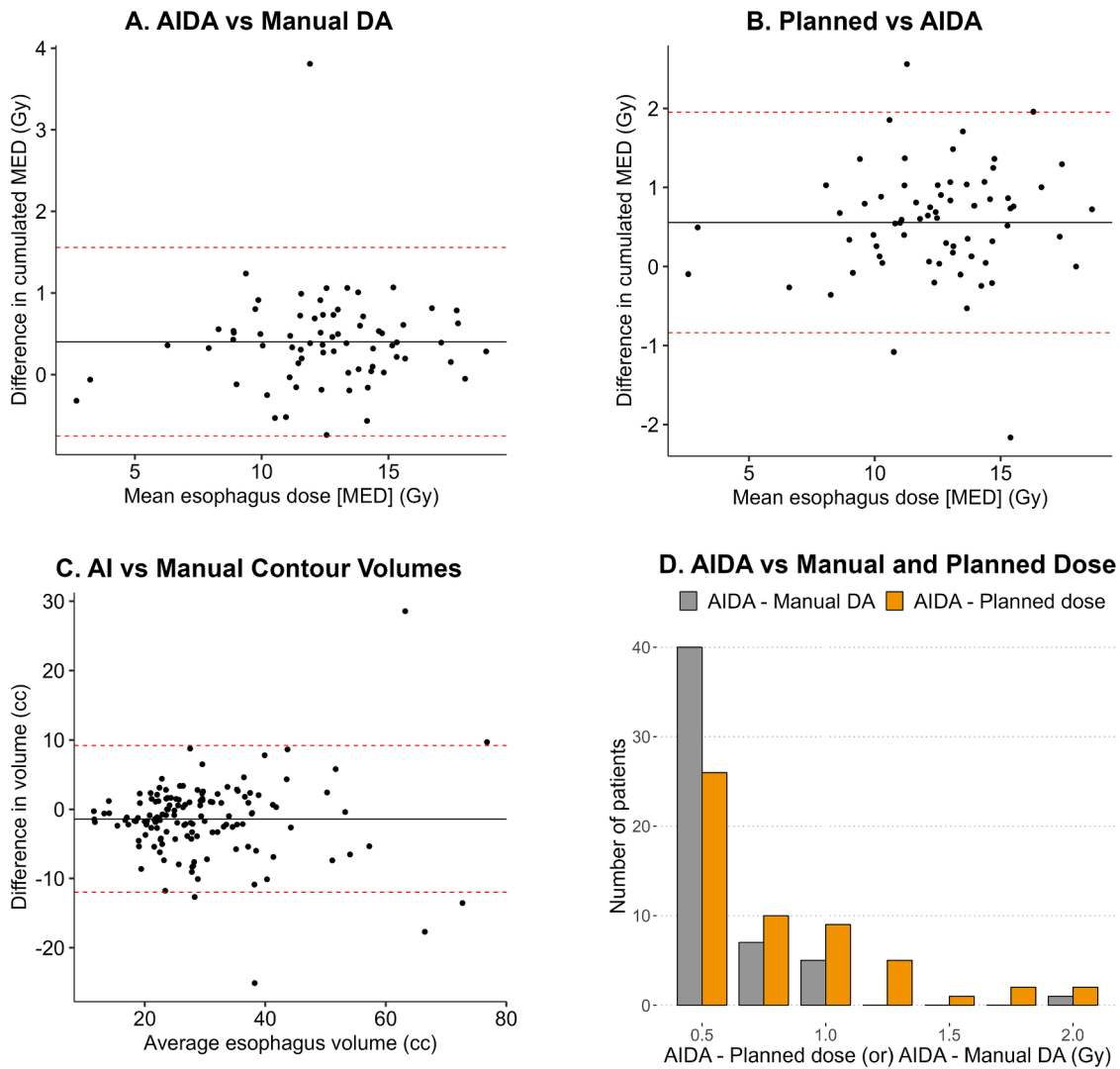


Fig. 2. Correlation between absolute MED deviations and DSC.



**Fig. 3.** Bland-Altman plots comparing A) the difference in cumulated MED between AIDA and manual DA and B) the difference in cumulated MED between AIDA and planned dose, C) in AI vs manually segmented volumes, and D) histogram of the number of patients with increasing dose deviations using absolute difference of AIDA and planned dose as well as AIDA and manual DA.

**3.2. AIDA-estimated cumulated MED closely matched those from manual DA across treatment weeks**

AIDA estimated  $MED_{w1}$  of  $6.4 \pm 1.6$  Gy and  $MED_{w2}$  of  $12.8 \pm 3.2$  Gy were slightly numerically higher than manual DA ( $MED_{w1}$  of  $6.2 \pm 1.6$  Gy and  $MED_{w2}$  of  $12.4 \pm 3.2$  Gy), but not significantly different ( $P = 0.4$  for both  $MED_{w1}$  and  $MED_{w2}$ ). SyN underestimated the doses compared to AIDA and manual DA ( $MED_{w1}$  of  $6.1 \pm 1.6$  Gy and  $MED_{w2}$  of  $12.2 \pm 3.1$  Gy). The planned  $MED_{w1}$  ( $6.1 \pm 1.5$  Gy) and the planned  $MED_{w2}$  ( $12.1 \pm 3.0$  Gy) were lower than manual DA and AIDA, but not significantly different than AIDA ( $P = 0.2$ ).

Bland-Altman analysis comparing AIDA-estimated cumulated MED with the cumulated planned MED showed a dose difference of 0.6 Gy with a range of  $-0.8$  Gy to  $2.0$  Gy (Fig. 3B), which was higher than the cumulated MED differences between AIDA and manual DA (Fig. 3A). Further, 40 patients had small, cumulated MED differences of below 0.5 Gy between AIDA and manual DA compared to 26 patients between AIDA and the planned dose (Fig. 3D). Similarly, 19 patients had dose differences exceeding 1 Gy between AIDA and planned dose compared to six patients when comparing AIDA and manual DA (Fig. 3D). Thus, smaller cumulated MED differences were observed between AIDA and manual DA than between AIDA and the planned dose.

**3.3. Fully automated estimation of mapped doses was similar to mapped doses when using manually edited AI-automated segmentation**

Fully automated AIDA esophagus and heart segmentations on the weekly CBCTs are shown for three representative patients in Fig. 4. Out of 11, one patient’s esophagus was excluded due to poor contrast on the CBCT. The segmentation agreement between the AIDA hearts and the manually edited hearts was  $DSC = 0.95 \pm 0.04$  and  $HD95 = 7.8 \pm 8.3$  mm in week 1, and  $DSC = 0.97 \pm 0.04$  and  $HD95 = 5.9 \pm 8.4$  mm in week 2. The corresponding results for automated vs. edited esophagus were  $DSC = 0.98 \pm 0.0$ ,  $HD95 = 0.5 \pm 0.7$  mm in week 1 and,  $DSC = 0.98 \pm 0.03$ ,  $HD95 = 0.7 \pm 1.3$  mm in week 2. There was no difference in MED and heart D90 between AIDA and the manually edited contours with average dose deviations less than 0.1 Gy ( $P > 0.05$ ).

**4. Discussion**

This study demonstrates the feasibility of an automated AI dose mapping framework for combined organ segmentation and RT dose mapping on weekly thoracic CBCTs exemplified primarily for the esophagus and the heart. Our analysis showed that AIDA produced similar estimates of dose as manual DA and the dose metrics were only

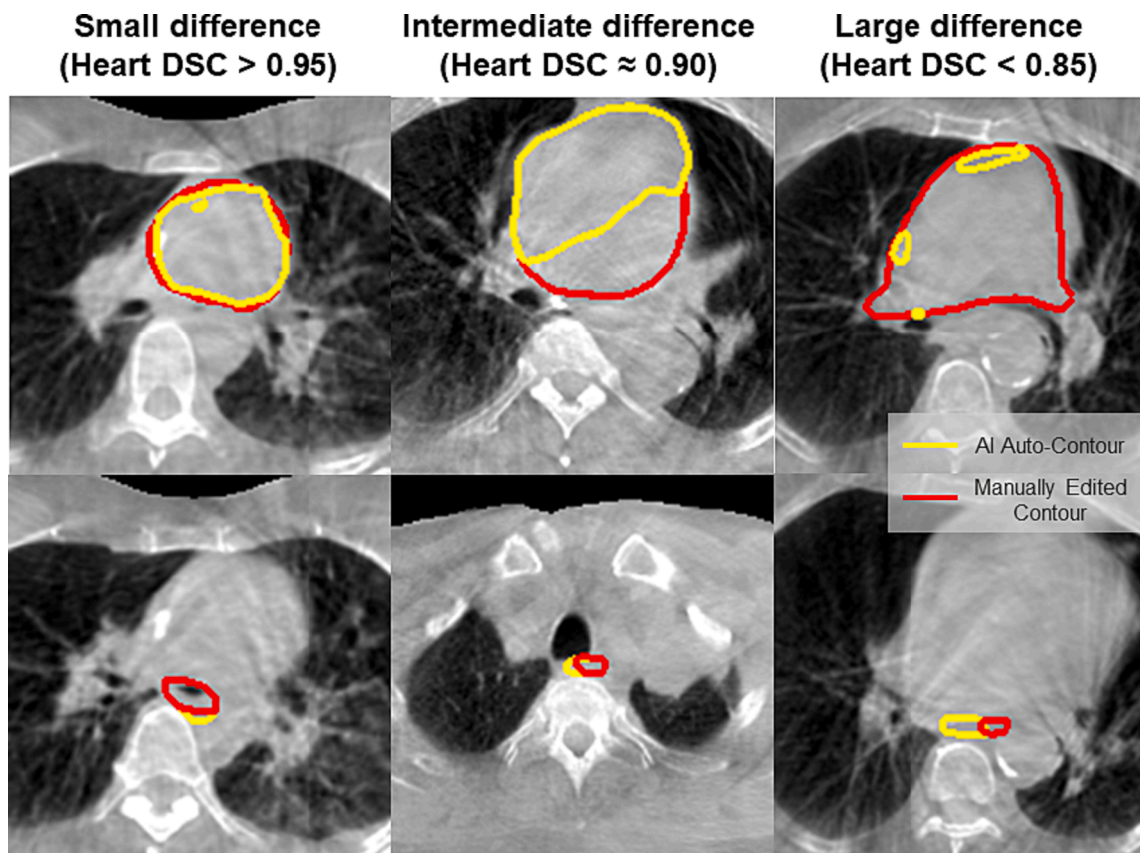


Fig. 4. Representative cases of AI auto-contour vs manually edited contour differences showing small, intermediate and, large differences selected based on the patients' heart DSCs.

weakly correlated to segmentation accuracy. Iterative SyN, on the other hand, was significantly less accurate and exhibited substantial deviations in dose compared to manual DA.

Importantly, our results harmonize with those from prior related studies [3,4] in that larger dose deviations ( $>1$  Gy in MED) were observed between the fully automated AIDA and planned doses compared to the AIDA and manual DA. Furthermore, a larger number of patients presented with small dose deviations ( $<0.5$  Gy in MED) between AIDA and manual DA, indicating that an AI-automated dose mapping is a feasible approach for thoracic normal tissues. Such methods, if available, would allow clinicians to objectively evaluate the quality of delivered radiation treatment plans and potentially adapt treatment to reduce treatment related toxicities when required.

Iterative DIR methods including the large deformation diffeomorphic metric mapping [3,11], geometry preserving methods (for CT to CT) [12] and biomechanical modeling [26] have provided highly accurate DIR even under large anatomical changes for RT mid-treatment assessments by using constraints including a rigid penalty to prevent unrealistic deformations of geometries. However, one highly observer-dependent and time-consuming limitation of such methods is the need for manual contouring of the relevant organs for mid-treatment CT and CBCT scans to produce diffeomorphic (or topology preserving) deformations, needed for optimization to enforce rigidity penalty of the organs of interest. The availability of AI automated segmentations reduces the need for manual delineation [27], albeit iterative registration methods still compute an iterative optimization with manual parameter tuning needed for each case [28]. Our approach, like other DL methods, computes fast registration without the need for any patient-specific tuning by directly regressing the transformation between image pairs.

Importantly, our method, like other current DL methods, was trained in an unsupervised manner without requiring ground truth DVFs, thus

simplifying network training [18,20,29,30]. However, a majority of DL methods make use of a small deformation framework to ensure faster and more stable training, which cannot preserve topology under large deformations [31–33], commonly occurring during RT due to changes in the tumor and nearby normal tissues (e.g. due to esophageal inflammation). Our PACS model overcomes this issue by computing progressively refined deformations and segmentation of organs on CBCTs [17]. We further extended the evaluation of PACS in a fully automated dose mapping framework, whereby the need for manual delineation even on pCT was eliminated by using a clinically used DL segmentation method [24].

There are a few limitations to this study. The fully automated AIDA was not evaluated for the lungs since the CBCT (FOV) did not fully encompass the lungs. Minor auto-segmentation defects were found in the slices with large imaging artifacts as well as in the superior and inferior regions of the esophagus and heart on the CBCTs, which improved CBCT image reconstruction approaches could potentially remedy. Secondly, the mid-phase for CBCT scans was employed for registration, and the study did not address the mitigation of breathing motion-induced artifacts which is a topic for future research. Additionally, the analyzed dataset was limited to the institutional dataset. Finally, the current use case examined dose mapping to obtain a rapid estimate of patients' prescribed doses. Hence, the extent of manual corrections needed for registration was not studied, which is more critical when the estimated RT doses are to be incorporated in adaptive plan re-optimization settings. Further studies are underway to extend this approach to other disease sites including the abdomen as well as external thoracic cancer datasets to evaluate the robustness of the AIDA approach.

In conclusion, an AI automated dose mapping framework that combines automated segmentation and deformable image registration-

based dose mapping for thoracic CBCTs was developed and evaluated. The segmentation and dose mapping results indicate the capability of AIDA to be used in a fully automated manner without the need for manual delineation of organs such as the esophagus and the heart.

### CRedit authorship contribution statement

**Jue Jiang:** Software, Formal analysis, Writing – original draft. **Chloe Min Seo Choi:** Software, Formal analysis, Writing – original draft. **Joseph O. Deasy:** Conceptualization. **Andreas Rimner:** Conceptualization, Resources. **Maria Thor:** Conceptualization, Methodology, Formal analysis, Investigation, Writing – original draft, Supervision. **Harini Veeraraghavan:** Conceptualization, Methodology, Formal analysis, Investigation, Writing – original draft, Supervision.

### Declaration of competing interest

The authors declare the following financial interests/personal relationships which may be considered as potential competing interests: This research was partially supported by the NCI R01CA258821-01 as well as the Memorial Sloan Kettering (MSK) Cancer Center Support Grant/Core Grant NCI P30CA008748. This research was also supported by a grant of the Korea Health Technology R&D Project through the Korea Health Industry Development Institute (KHIDI), funded by the Ministry of Health & Welfare, Republic of Korea (grant number: HI19C1234).

### Acknowledgments

This research was partially supported by the NCI R01CA258821-01 as well as the Memorial Sloan Kettering (MSK) Cancer Center Support Grant/Core Grant NCI P30CA008748.

This research was supported by a grant from the Korea Health Technology R&D Project through the Korea Health Industry Development Institute (KHIDI), funded by the Ministry of Health & Welfare, Republic of Korea (grant number: HI19C1234).

### References

- Zhang P, Yorke E, Hu Y-C, Mageras G, Rimner A, Deasy JO. Predictive treatment management: incorporating a predictive tumor response model into robust prospective treatment planning for non-small cell lung cancer. *Int J Radiat Oncol Biol Phys* 2014;88:446–52.
- Sonke J-J, Belderbos J. Adaptive radiotherapy for lung cancer. *Semin Radiat Oncol* 2010;20:94–106.
- Alam SR, Zhang P, Zhang SY, Chen I, Rimner A, Tyagi N, et al. Early Prediction of Acute Esophagitis for Adaptive Radiation Therapy. *Int J Radiat Oncol Biol Phys* 2021;110:883–92. <https://doi.org/10.1016/j.ijrobp.2021.01.007>.
- Luo J, Ma C, Yu S, Li Z, Ma C. Study of the Cumulative Dose Between Fractions of Lung Cancer Radiotherapy Based on CT and CBCT Image Deformable Registration Technology. *Frontiers. Physics*. 2020;8. <https://doi.org/10.3389/fphy.2020.00021>.
- Thor M, Apte A, Haq R, Iyer A, LoCastro E, Deasy JO. Using Auto-Segmentation to Reduce Contouring and Dose Inconsistency in Clinical Trials: The Simulated Impact on RTOG 0617. *Int J Radiat Oncol Biol Phys* 2021;109:1619–26.
- Jaffray DA, Lindsay PE, Brock KK, Deasy JO, Tomé WA. Accurate accumulation of dose for improved understanding of radiation effects in normal tissue. *Int J Radiat Oncol Biol Phys* 2010;76:S135–S139.
- Chetty IJ, Rosu-Bubulac M. Deformable Registration for Dose Accumulation. *Semin Radiat Oncol* 2019;29:198–208.
- Zhang P, Rimner A, Yorke E, Hu Y-C, Kuo L, Apte A, et al. A geometric atlas to predict lung tumor shrinkage for radiotherapy treatment planning. *Phys Med Biol* 2017;62:702–14.
- Zhang P, Yorke E, Mageras G, Rimner A, Sonke JJ, Deasy JO. Validating a Predictive Atlas of Tumor Shrinkage for Adaptive Radiotherapy of Locally Advanced Lung Cancer. *Int J Radiat Oncol Biol Phys* 2018;102:978–86. <https://doi.org/10.1016/j.ijrobp.2018.05.056>.
- Court LE, Tucker SL, Gomez D, Liao Z, Zhang J, Kry S, et al. A technique to use CT images for in vivo detection and quantification of the spatial distribution of radiation-induced esophagitis. *J Appl Clin Med Phys* 2013;14:4195.
- Alam S, Thor M, Rimner A, Tyagi N, Zhang S-Y, Kuo LC, et al. Quantification of accumulated dose and associated anatomical changes of esophagus using weekly Magnetic Resonance Imaging acquired during radiotherapy of locally advanced lung cancer. *Phys Imaging Radiat Oncol* 2020;13:36–43.
- Guy CL, Weiss E, Christensen GE, Jan N, Hugo GD. CALIPER: A deformable image registration algorithm for large geometric changes during radiotherapy for locally advanced non-small cell lung cancer. *Med Phys* 2018;45:2498–508.
- Bosma LS, Ries M, Denis de Senneville B, Raaymakers BW, Zachiu C. Integration of operator-validated contours in deformable image registration for dose accumulation in radiotherapy. *Phys Imaging. Radiat Oncol*. 2023;27. 100483.
- Alam S, Veeraraghavan H, Tringale K, Amoateng E, Subashi E, Wu AJ, et al. Inter-intrafraction motion assessment and accumulated dose quantification of upper gastrointestinal organs during magnetic resonance-guided ablative radiation therapy of pancreas patients. *Phys Imaging Radiat Oncol* 2022;21:54–61. <https://doi.org/10.1016/j.phro.2022.02.007>.
- Han X, Hong J, Reingold M, Crane C, Cuaron J, Hajj C, et al. Deep-learning-based image registration and automatic segmentation of organs-at-risk in cone-beam CT scans from high-dose radiation treatment of pancreatic cancer. *Med Phys* 2021;48:3084–95. <https://doi.org/10.1002/mp.14906>.
- Li Kuan Ong A, Knight K, Panettieri V, Dimmock M, Kit Loong Tuan J, Qi Tan H, et al. Predictors for late genitourinary toxicity in men receiving radiotherapy for high-risk prostate cancer using planned and accumulated dose. *Phys Imaging Radiat Oncol* 2023;25:100421.
- Jiang J, Veeraraghavan H. One shot PACS: Patient specific Anatomic Context and Shape prior aware recurrent registration-segmentation of longitudinal thoracic cone beam CTs. *IEEE Trans Med Imaging* 2022;PP.. <https://doi.org/10.1109/TMI.2022.3154934>.
- de Vos BD, Berendsen FF, Viergever MA, Sokooti H, Staring M, Išgum I. A deep learning framework for unsupervised affine and deformable image registration. *Med Image Anal* 2019;52:128–43.
- Fu Y., Lei Y., Liu Y., Wang T., Curran W.J., Liu T., et al. Cone-beam Computed Tomography (CBCT) and CT image registration aided by CBCT-based synthetic CT. *Medical Imaging 2020: Image Processing*, vol. 11313, SPIE; 2020, p. 721–7. <https://doi.org/10.1117/12.2549095>.
- Balakrishnan G, Zhao A, Sabuncu MR, Guttag J, Dalca AV. VoxelMorph: A Learning Framework for Deformable Medical Image Registration. *IEEE Trans Med Imaging* 2019. <https://doi.org/10.1109/TMI.2019.2897538>.
- Lee D, Alam SR, Jiang J, Zhang P, Nadeem S, Hu Y-C. Deformation driven Seq2Seq longitudinal tumor and organs-at-risk prediction for radiotherapy. *Med Phys* 2021; 48:4784–98.
- Avants BB, Epstein CL, Grossman M, Gee JC. Symmetric diffeomorphic image registration with cross-correlation: evaluating automated labeling of elderly and neurodegenerative brain. *Med Image Anal* 2008;12:26–41.
- Tustison NJ, Avants BB. Explicit B-spline regularization in diffeomorphic image registration. *Front Neuroinform* 2013;7:39.
- Um H, Jiang J, Thor M, Rimner A, Luo L, Deasy JO, et al. Multiple resolution residual network for automatic thoracic organs-at-risk segmentation from CT. *arXiv [eessIV]* 2020. 10.48550/ARXIV.2005.13690.
- Kollmannsberger P, Kerschnitzki M, Repp F, Wagermaier W, Weinkamer R, Fratzl P. The small world of osteocytes: connectomics of the lacuno-canalicular network in bone. *New J Phys* 2017;19:073019.
- Veleg M, Juang T, Moseley JL, Oldham M, Brock KK. Utility and validation of biomechanical deformable image registration in low-contrast images. *Pract Radiat Oncol* 2015;5:e401. e408.
- McCulloch MM, Cazoulat G, Svensson S, Gryshkevych S, Rigaud B, Anderson BM, et al. Leveraging deep learning-based segmentation and contours-driven deformable registration for dose accumulation in abdominal structures. *Front Oncol* 2022;12:1015608.
- Chen Y, Yin F-F, Jiang Z, Ren L. Daily edge deformation prediction using an unsupervised convolutional neural network model for low dose prior contour based total variation CBCT reconstruction (PCTV-CNN). *Biomed Phys Eng Express* 2019; 5. <https://doi.org/10.1088/2057-1976/ab446b>.
- Mok TCW, Chung A. Fast symmetric diffeomorphic image registration with convolutional neural networks. *Proceedings of the IEEE/CVF conference on computer vision and pattern recognition*. 2020. 4644–53.
- Fu Y, Wang T, Lei Y, Patel P, Jani AB, Curran WJ, et al. Deformable MR-CBCT prostate registration using biomechanically constrained deep learning networks. *Med Phys* 2021;48:253–63.
- Mok TCW, Chung ACS. Large Deformation Diffeomorphic Image Registration with Laplacian Pyramid Networks. *Medical Image Computing and Computer Assisted Intervention – MICCAI 2020*. Springer International Publishing; 2020. 211–21.
- Niethammer M, Kwitt R, Vialard F-X. Metric Learning for Image Registration. 2019 IEEE/CVF Conference on Computer Vision and Pattern Recognition (CVPR) 2019. 10.1109/cvpr.2019.00866.
- Ashburner J. A fast diffeomorphic image registration algorithm. *Neuroimage* 2007; 38:95–113.